GA–A26774

DUST APPEARANCE RATES DURING NEUTRAL BEAM INJECTION AND AFTER OXYGEN BAKE IN THE DIII-D TOKAMAK

by
J.H. YU, R.D. SMIRNOV, D.L. RUDAKOV

JULY 2010

GENERAL ATOMICS

DISCLAIMER

GA–A26774

DUST APPEARANCE RATES DURING NEUTRAL BEAM INJECTION AND AFTER OXYGEN BAKE IN THE DIII-D TOKAMAK

by
J.H. YU*, R.D. SMIRNOV*, D.L. RUDAKOV*

This is a preprint of a paper to be presented at the Nineteenth International Conference on Plasma Surface Interactions, May 24-28, 2010, in San Diego, California, and to be published in the *J. Nucl. Mater.*

*University of California San Diego, San Diego, California.

Work supported by
the U.S. Department of Energy
under DE-FG02-07ER54917, DE-FC02-04ER54698, and DE-FG02-04ER54852

GENERAL ATOMICS ATOMICS PROJECT 30200
JULY 2010

GENERAL ATOMICS

ABSTRACT

A simple model to quantify source and sink terms of dust observed in tokamaks using fast visible imaging is presented. During neutral beam injection (NBI), dust appearance rates increase in front of the neutral beam port by up to a factor of 5. The images show dust streaming from the port box as previously settled dust becomes mobilized during beam injection. Following an oxygen bake and vent, the dust observation rate is a factor of 2 lower than that after a vessel entry vent with no oxygen bake. Detected dust levels decay on a shot-to-shot basis in a roughly exponential fashion, with a decay time of approximately 20 sec of plasma exposure. Appearance rates of dust mass are estimated using assumed lognormal and power law functional forms for the dust size distribution. The two dust size distributions differ significantly on the amount the dust material carried by the largest particles, highlighting the need for further dust studies in order to make accurate forecasts to ITER.

I. INTRODUCTION

Dust is an important issue for future tokamaks because of safety issues such as tritium retention and the possibility of explosion hazard when dust is accidentally exposed to air and water [1]. Core and scrape-off-layer (SOL) contamination of the plasma by dust may also be a concern because ablated dust is a source of impurities which affects plasma performance. Studies of dust in DIII-D include the use Nd:YAG lasers [2] that detect scattered light from dust particles ranging in size from 0.1 – 1.6 μm, which is estimated using a model based on Mie scattering [3]. This class of particles detected with laser scattering is smaller than the particles detected with cameras, which can detect particles with radii larger than approximately 2 to 3 μm [4]. Note that typical optics used with existing cameras do not actually resolve particles this small; rather thermal emission from the hot particle surface, or for sufficiently hot and dense plasma, line radiation from the ablation plume surrounding the particle, is detected. Cameras have been used elsewhere to study dust, including the use of multiple cameras to determine 3D dust trajectories [5]. Here we present a simple model to infer the source and sink terms for the dust appearance rate using fast visible imaging, and apply the model to dust detected during neutral beam injection (NBI). In addition, a model to estimate the mass appearance rate of dust is presented and applied to startup plasmas following the recent DIII-D oxygen bake and vent. The results are valid for the relatively large (> a few microns) particles detected by fast cameras.

II. EXPERIMENTAL SETUP AND IMAGE ANALYSIS

Imaging data is obtained with a fast visible camera that has a tangential view of ~ 6 m^3 in the midplane region of the DIII-D tokamak vessel. An objective lens focuses light onto the front face of an 8×10 mm coherent fiber-optic bundle, and light coming out the back of the fiber bundle is focused onto a Phantom v7.1 CMOS camera detector with 12 bit pixel depth. The spatial resolution of the detector is 384×256 pixels with 1 pixel imaging approximately 0.2 cm^2 at the point of tangency. The images presented here are obtained without an optical filter, and the camera optical system detects wavelengths in the range of 450 to 950 nm. The frame rates range from 1×10^3 to 5×10^3 frames/s, and each plasma discharge typically consists of $> 10^4$ frames. Additional details of the fast camera system are found in [6].

Each camera pixel views a line-integrated volume along the line of sight coordinate s. The total volume of the scrape-off-layer (SOL) viewed by the camera is $V_{SOL,cam} = \sum \int_{SOL} \Omega s_i^2 ds_i \approx 1$ m^3. Here $\Omega = 3.2 \times 10^{-6}$ steradian is the solid angle subtended by each pixel's line of sight, $\int_{SOL}$ denotes that only line of sight segments in the SOL contribute to the integral, and the discrete sum is over all i pixels in the frame.

The images are processed to maximize the probability of detecting dust particles. For each camera frame, a background image is subtracted to remove wall features, reflections, and the steady state plasma emission. Typically 10 frames corresponding to nearly the same time as the frame of interest are averaged to create the background image. After background subtraction, the image is further processed with a 2D Gaussian filter to enhance dust particles within the frame. Brightness and size criteria are used to identify dust particles in each frame. Particles are then tracked from frame to frame by considering all possible identifications of the particle positions with the particle positions in the subsequent frame. Particles are identified as being the same particle from frame to frame by minimizing the total squared displacement from one frame to the next, and by taking into account user-defined restrictions such as the maximum allowed displacement a particle can make between frames. An example of this detection method is shown in Fig. 1, along with the unprocessed image. The detection algorithm detects most particles but not all, and in some cases detects features that are not actual particles. The typical error rate is $< 30\%$.

In each frame the total number of dust particles N_{tot} is recorded. The number of new particles N_n detected in each frame is determined by decomposing N_{tot} into two parts, $N_{tot} = N_s + N_n$. Here N_s is the number of surviving particles in the frame of interest, where a surviving particle is identified as existing in the previous frame as determined by tracking individual particles from frame to frame. Since we are interested in source and

sink terms for dust appearance rates, breaking up N_{tot} is necessary to prevent counting the same particle multiple times from frame to frame.

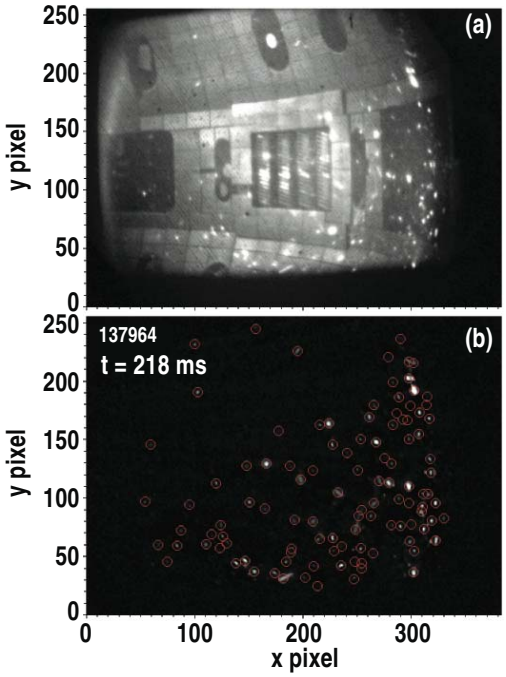

Fig. 1. (a) The camera view inside DIII-D during with unusually high dust levels due to intentionally introduced dust in a previous discharge. (b) Example of dust grain detection in the same frame as shown in (a), after background subtraction.

III. MODEL OF DETECTED DUST SOURCE AND SINK TERMS

We assume a uniform dust density in the SOL and assume no dust exists elsewhere, such that

$$n_d(R) = \begin{Bmatrix} \overline{n_d}, & R_{sep} < R < R_w \\ 0, & else \end{Bmatrix} \quad , \tag{1}$$

where R_{sep} and R_w are the major radii of the separatrix and outer wall, respectively, and the average dust density detected by the camera is $\overline{n_d} = N_{tot}/V_{SOL,cam}$. The discretized continuity equation in the SOL is then simply $\frac{1}{\Delta t}\left[\overline{n_d}(t) - \overline{n_d}(t-\Delta t)\right] = P - L$, where Δt is the time between frames. The ability to track individual particles and separately obtain N_n and N_s allows us to write approximations for the detected dust density source and sink terms as

$$P = \frac{N_n(t)}{V_{SOL,cam}\Delta t} \text{ and } L = \frac{N_{tot}(t-\Delta t) - N_s(t)}{V_{SOL,cam}\Delta t} \quad , \tag{2}$$

respectively.

IV. DUST INCREASE DURING NBI

To apply this formalism to actual data, a relatively large amount of dust is needed to obtain good statistics. We use a plasma discharge immediately following an attempted discharge in which loose dust was injected using the Divertor Materials Evaluation System (DIMES) [7]. The camera measures a precipitous increase in the dust appearance rate during NBI in discharge 136457 (lower single null, 0.7 MA plasma current, $B_T = 2.0$ T). Increased dust levels during NBI have also been reported using laser detection [8]. For the data presented here, the increase in observable dust particles is predominantly due to mobilization and heating of dust that has previously settled on the bottom surface of the NBI port. The dashed line in Fig. 2 shows that the total number of dust particles detected with the camera in each frame increases by a factor of ~ 5 during NBI compared to no NBI. The dust density source and sink terms given by Eq. 2 are shown as the red and orange lines, and both increase by a factor of ~ 3 during NBI. Taking the difference between the source and sink terms gives the approximate instantaneous rate of change of the observed dust density, i.e. $\partial n_d / \partial t \approx P - L$, shown as the blue line. The delay between the source and sink terms is the average duration of dust visibility. Most particles that are mobilized during NBI become ablated when they reach the separatrix. In general, decoding whether the dust disappearance, or loss term L, is due to dust ablation, particles leaving the camera field of view, or particles cooling so that they are no longer visible, is a challenging problem and is not addressed here.

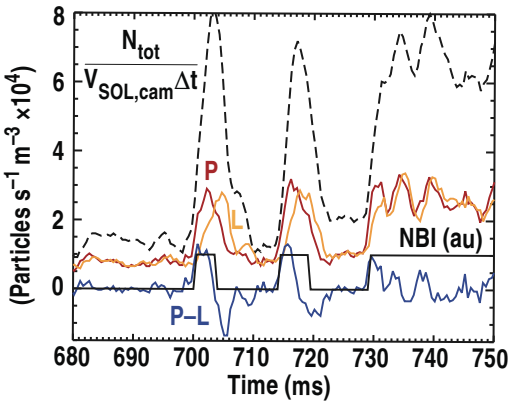

Fig. 2. Dust source (P) and sink (L) terms shown as the red and orange lines, respectively, with and without NBI (black solid line). P and L are calculated from total number of detected particles in each frame (black dashed line). Rate of change of dust density is shown as blue line.

V. MODEL OF DUST MASS APPEARANCE RATE

The mass of the observed dust is calculated by taking the third moment of the dust size distribution function $f(R_d)$ and using an assumed dust mass density of $\rho = 2$ g/cm^3 for carbon. The mass appearance rate is given by

$$r_{mass}(t) = \int_{SOL} P\Omega s^2 4/3\pi\rho \int_{R_{d\min}(s)}^{R_{d\max}} R_d{}^3 f(R_d) dR_d ds \quad . \tag{3}$$

The minimum observable particle size $R_{d\min}$ is a function of the distance s between the dust particle and camera objective lens. For dust particles with an image area smaller than the area of a pixel, the camera signal from thermal radiation from the dust particle is proportional to the particle's radius squared and is inversely proportional to s^2 [9]. The combination of these effects results in $R_{d\min}$ being approximately linearly proportional to s. In general, $R_{d\min}$ is a function of the plasma density n_e and electron temperature T_e; here we use $R_{d\min} = 4\times10^{-6} s$ based on approximate values of $n_e \approx 5\times10^{12}$ cm^{-3} and $T_e \approx 20$ eV in the SOL, and constrained by the lower limit of observable dust size determined with calibrated dust injection [4].

VI. DUST SIZE DISTRIBUTION

A lognormal and a power law distribution are modeled, and the size distributions are normalized such that $\int_{R_{d\min}(s_{\min})}^{R_{d\max}} f(R_d)dR_d = 1$, where $s_{\min} \approx 0.5$ m is the minimum distance from the camera objective lens to the SOL region. The lognormal distribution is

$$f(R_d) = \frac{a}{R_d}\exp\left[-\frac{(\ln R_d - \ln R_o)^2}{2\ln^2 \sigma_g}\right] , \quad (4)$$

and the power law distribution is $f(R_d) = bR_d{}^{\alpha}$, where a and b are normalization coefficients. In Eq. 4, R_o is the geometric mean and σ_g is the geometric standard deviation.

The parameters of the size distributions are constrained by studies of collected dust and by estimates of dust size in DIII-D using imaging, based on the observed dust particle lifetime and theoretical ablation rate of a carbon sphere [4]. The imaging data are shown as squares in Fig. 3, and size measurements from dust collected in ASDEX are shown as diamonds for reference [10], with the data sets normalized at $R_d = 2$ μm. The study of collected dust in ASDEX provided the most detail on the actual size distribution data, which is why it was chosen here. However, the collected dust consists of particles surviving on and under the surfaces, which is not necessarily representative of dust found in the plasma. The size distribution of the collected dust in ASDEX roughly follows a lognormal distribution, but caution should be used when applying this distribution to in situ dust detection. Depending on the collection location, the collected dust in ASDEX has median count diameters ranging from 1.4 to 5.5 μm with an average value of 3.3 μm, and geometrical standard deviations ranging from σ_g = 2.5 to 4.0. These values are fairly typical of other tokamaks [11, 12], although DIII-D reports smaller collected dust sizes [13].

As shown in Fig. 3, a lognormal fit to the data yields $R_o = 1.1$ μm and σ_g = 3.4, and a power law fit to the imaging data yields $\alpha = -1.6$. These two size distributions will be used in the remainder of the paper. We limit the upper range of the dust size integral in Eq. 3 to a realistic size of $R_{d\max}$ = 100 μm based on collected dust samples. The sizes of the largest particles previously inferred through imaging are most likely overestimated, since vapor shielding effects become significant for large R_d [14].

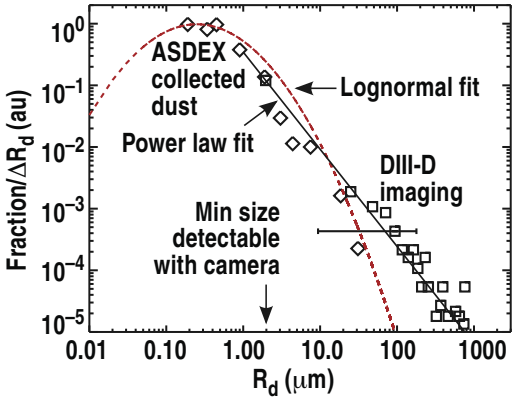

Fig. 3. Dust size distribution based on dust collected in ASDEX (diamonds) and imaging in DIII-D (squares). Lognormal and power law fits to the data are shown as dashed and solid lines, respectively.

VII. DUST MASS APPEARANCE RATES AFTER OXYGEN BAKE

Oxygen baking has been proposed for ITER as a method of controlling the in-situ tritium inventory by removing co-deposited tritium from the walls. DIII-D was recently baked at a temperature of 350°C using a 10 Torr fill of a 20% O_2 - 80% He mixture. Dust levels were measured with the fast camera in plasma discharges immediately after the oxygen bake and vent.

We numerically solve the integrals in Eq. 3 to determine the shot-averaged dust mass appearance rate $\bar{r}_{mass}$, calculated with the shot-averaged dust source term $\bar{P} = N_n^{(shot)} / \left(\tau V_{SOL,cam} \right)$ using the number of detected new particles $N_n^{(shot)}$ throughout the discharge, and where τ is the discharge duration. For the relatively low dust appearance rates here, $N_n^{(shot)}$ is determined by manually counting particles. In the camera-viewable region of the tokamak (~ 1 m^3 SOL volume, and ~ 6 m^3 of total vessel volume), the average dust count rate for the first plasma discharge 142758 after the oxygen bake is 160 particles/sec, while for 136457 (Fig. 2) following intentional dust injection the dust count rate is as high as a few $\times 10^4$ particles/sec; during normal operations the average rate of dust observation is < 5 particles/sec. The dust observation rate varies somewhat throughout a typical discharge, with highest levels typically at the beginning and end of the discharge.

Figure 4 shows the exponential decay of the dust mass appearance rate versus the cumulative duration of plasma discharges following the oxygen bake and vent. The plasma discharges shown here range from ohmic to H-mode, with plasma current 0.9 to 1.2 MA, and $B_T = 1.7$ T. The two dust size distributions differ significantly on amount the dust material carried by the largest particles, with the power law distribution yielding a mass appearance rate that is more than an order of magnitude higher than the lognormal distribution. Following the vent and oxygen bake, the decay time of the detected dust rate is 22 sec of plasma exposure. This decay time is a factor of 2 longer, and the initial level of detected dust is a factor of 2 lower, compared with discharges (beginning with 135992) following a manned vessel entry with no oxygen bake. The levels of dust following a manned entry are typically high due to dust that is unintentionally brought into the vessel. The vessel clean-up timescale, characterized by the dust decay time, presumably depends on plasma parameters and magnetic configuration. Assuming dust is composed of carbon, initial post-vent appearance rates in the camera field of view for dust mass following the oxygen bake and vent are estimated using lognormal and power law dust size distributions, yielding ~ 3 μg/sec and ~ 50 μg/sec, respectively. Not surprisingly, the estimated mass appearance rate from the power law distribution is extremely sensitive to the upper range of the dust size integral, $R_{d\,\max}$.

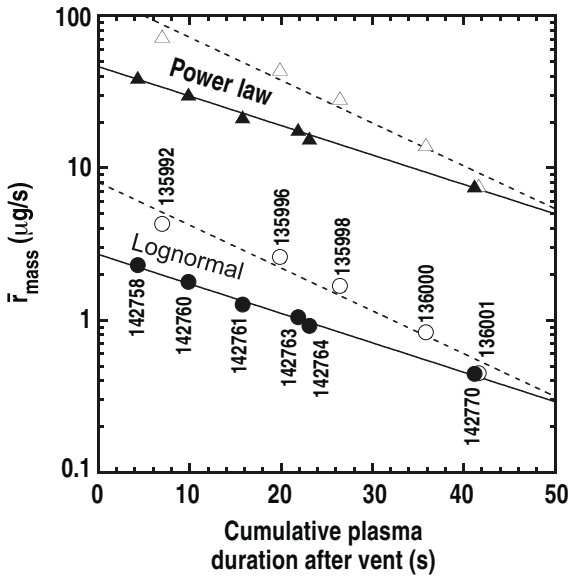

Fig. 4. Shot-averaged mass appearance rates $\bar{r}_{mass}$ calculated for carbon dust after a vent with oxygen bake (solid data points) and after a vessel entry with no bake (open points), using both lognormal (circles) and power law (triangles) size distributions. The solid and dashed lines are exponential fits.

Figure 4 neglects dust produced during disruptions, which occurred in most of the discharges analyzed, because the quantity of dust generated by these abrupt plasma material interactions varies from shot to shot. Typically dust is generated during disruptions with vertical displacement events. The largest observed dust production during disruptions for these discharges occurred at the end of 142764, which resulted in a dust observation rate of $\sim 1 \times 10^4$ particles/sec during the ~ 20 ms duration of the current quench.

VIII. CONCLUSIONS

Based on the assumption of uniform dust density in the SOL, a simple model using a statistical approach is presented that quantifies source and sink terms of dust observed using fast visible imaging. This model is extended to estimate the mass of detected dust, using assumed dust size distributions. Power law and lognormal dust size distributions differ significantly on the amount the dust material carried by the largest particles, which demonstrates the need for further study of dust statistics in tokamaks so that accurate forecasts to ITER can be made.

Dust observation rates increase by up to a factor of 5 during NBI as particles are observed to move out of the beam port box and into the SOL, where they subsequently disappear when ablated. Dust observation rates following an oxygen bake and a vent are a factor of 2 lower than those after a vessel entry with no oxygen bake. The decay time for the appearance level of post-vent dust ranges from approximately 10 to 20 sec of plasma exposure.

REFERENCES

[1] G. Federici, *et al.*, Nucl. Fusion **41** (2001) 1967.

[2] W.P. West, *et al.*, Plasma Phys. Control. Fusion **48** (2006) 1661.

[3] R.D. Smirnov, *et al.*, Phys. Plasmas **14** (2007) 112507.

[4] J.H. Yu, *et al.*, J. Nucl. Mater. **390–391** (2009) 216.

[5] A.L. Roquemore, *et al.*, J. Nucl. Mater. **363-365** (2007) 222.

[6] J.H. Yu and M.A. Van Zeeland, Rev. Sci. Instrum. **79** (2008) 10F516.

[7] D.L. Rudakov, *et al.*, Nucl. Fusion **49** (2009) 085022.

[8] W.P. West, B.D. Bray, J. Nucl. Mater. **363–365** (1007) 107.

[9] R.D. Smirnov, *et al.*, Plasma Phys. Control. Fusion **51** (2009) 055017.

[10] J.P. Sharpe, D.A. Petti, and H.-W. Bartels, Fusion Eng. Des. **63-64** (2002) 153.

[11] Sharpe, J. Nucl. Mater. **313–316** (2003) 455.

[12] Ph. Chappuis, *et al.*, J. Nucl. Mater. **290 -293** (2001) 245.

[13] W.J. Carmack, *et al.*, Fusion Eng. Design **39–40** (1998) 477.

[14] S.I. Krasheninnikov, *et al.*, Plasma Phys. Control. Fus. **50** (2008) 124054.

ACKNOWLEDGMENT

The authors would like to thank M.A. Van Zeeland for contributing to writing code, and N. Brooks for useful discussions. This work supported by the U.S. Department of Energy under DE-FG02-07ER54917, DE-FC02-04ER54698, and DE-FG02-04ER54852.